npj | climate and atmospheric science

www.nature.com/npjclimatsci

ARTICLE OPEN

Check for updates

Trends and oscillations in arctic mediterranean atmospheric static stability during recent arctic warming

Xin Wang[1] and Jinping Zhao[1,2]✉

The long-term variation in the static stability of lower atmosphere (SSLA) in the Arctic Mediterranean is investigated using reanalysis data. Climatological SSLA is categorized into a high-value region (Polar Region) and two low-value regions in the Norwegian Sea (Region-A) and southern part of Iceland (Region-B). The variations of SSLA are divided into trends and oscillations. In the Polar Region, SSLA exhibited a decreasing trend due to Arctic warming and sea ice decline, with negligible oscillatory variations. In Region-A and Region-B, the trends of SSLA are insignificant, while the oscillatory variation becomes obvious. SSLA there are highly correlated to Arctic Oscillation (AO) Index and vertical velocity. The driving factors in weakening SSLA are vertical velocity and surface heating, related to enhanced warm water advection dominated by AO. The variation of SSLA in turn feeds back the vertical velocity and AO.

npj Climate and Atmospheric Science (2024)7:27 ; https://doi.org/10.1038/s41612-024-00576-7

INTRODUCTION

Static stability is determined by the vertical distributions of the atmospheric temperature and humidity, and refers to the ability of an air mass to return to its original equilibrium position after moving vertically[1–5]. It is a fundamental physical parameter closely linked to convective activities[5–8] and widely used to describe the atmospheric state[1,2,6,9]. Previous research has established that the static stability has an important effect on mesoscale and large-scale atmospheric processes[5,10–17]. Variations of static stability affects the local atmosphere and climate: it influences the oscillation frequency of vertical perturbations[6], internal waves[18], gravitational waves[19], wave-generated flow[20], cloud cover[16,17,21–24] and cyclone systems[10,25,26].

In the Arctic, many studies focus on the positive correlation between the static stability of lower atmospheric (SSLA) and the Arctic cloud cover[17,22,23,27,28], which plays important role for energy budget in the Arctic[29,30]. The static stability is experiencing obvious variations due to the Arctic warming and sea ice retract[15,31–37]. Models and reanalysis data have also been employed to investigate the response of static stability to sea ice loss[38–40].

The relationship between static stability and the Arctic Oscillation (AO) is important but relatively underexplored. AO is defined as the first mode of the Empirical Orthogonal Function of SLP north of 20°N, and the time coefficient of this mode was referred to as the Arctic Oscillation Index[41]. The AO is the most important pattern of atmospheric circulation in Northern Hemisphere, especially in winter[42,43]. North Atlantic Oscillation (NAO) is another index highly correlated with AO[44,45]. Here we use AO to present both AO and NAO. It is necessary to investigate the relationship between atmospheric static stability and AO to better understand the mechanism influencing the Arctic climate system.

This study investigates the trends and oscillatory changes of SSLA in the Arctic Mediterranean. Additionally, it explores the connection between the AO and SSLA. This paper reveals the driving factor behind SSLA variations and discusses the importance of SSLA in the Arctic Oscillation system. Consistent with previous research[16,24,32,46–48], we calculated the average of the 925 and 850 hPa levels to represent the lower atmosphere in this study.

RESULTS

For this study, three datasets (NCEP-R2, ERA5, and JRA-55) were employed to ensure the robustness of the results and to assess sensitivity to dataset choice. In the majority of cases, the results were comparable, and we present only the NCEP-R2 results, except in instances where results from different datasets significantly diverge.

Seasonal variation in static stability of the lower atmosphere in the Arctic Mediterranean

Throughout this paper, N^2 is used to present the value of SSLA (see Methods for details). The SSLA exhibits conspicuous seasonal variations and spatial differences, as illustrated in Fig. 1. Analyzing the annual cycle, the spatial distribution of SSLA in the Arctic Mediterranean can be broadly categorized into winter and summer patterns, with transitional patterns observed in spring and autumn.

In winter (December-March), the majority of the Arctic Ocean exhibits high values (greater than $3.3 \times 10^{-4}\,s^{-2}$), whereas the Norwegian Sea and the area south of Iceland manifest low values (below than $2.0 \times 10^{-4}\,s^{-2}$). Threshold values are determined by identifying the outermost isolines among the densely concentrated isolines, effectively delineating regions with high and low SSLA values. The high SSLA in the Arctic Ocean is distinctly linked to the presence of underlying sea ice. This phenomenon induces a stable boundary layer characterized by surface-based inversions, driven by a substantial deficit in surface net radiation over the snow and ice surface during the polar night[49–52], consequently resulting in an increase in SSLA.

The SSLA in the Norwegian Sea is primarily associated with its underlying warm surface, dominated by the Norwegian Atlantic Current[53]. In the area south of Iceland, SSLA is influenced by the recirculation area of the North Atlantic Current[54]. Both areas remain ice-free due to the warmer water transported by the

[1]Ocean University of China, Qingdao, China. [2]Key Laboratory of Physical Oceanography. MOE. China, Qingdao, China. ✉email: jpzhao@ouc.edu.cn

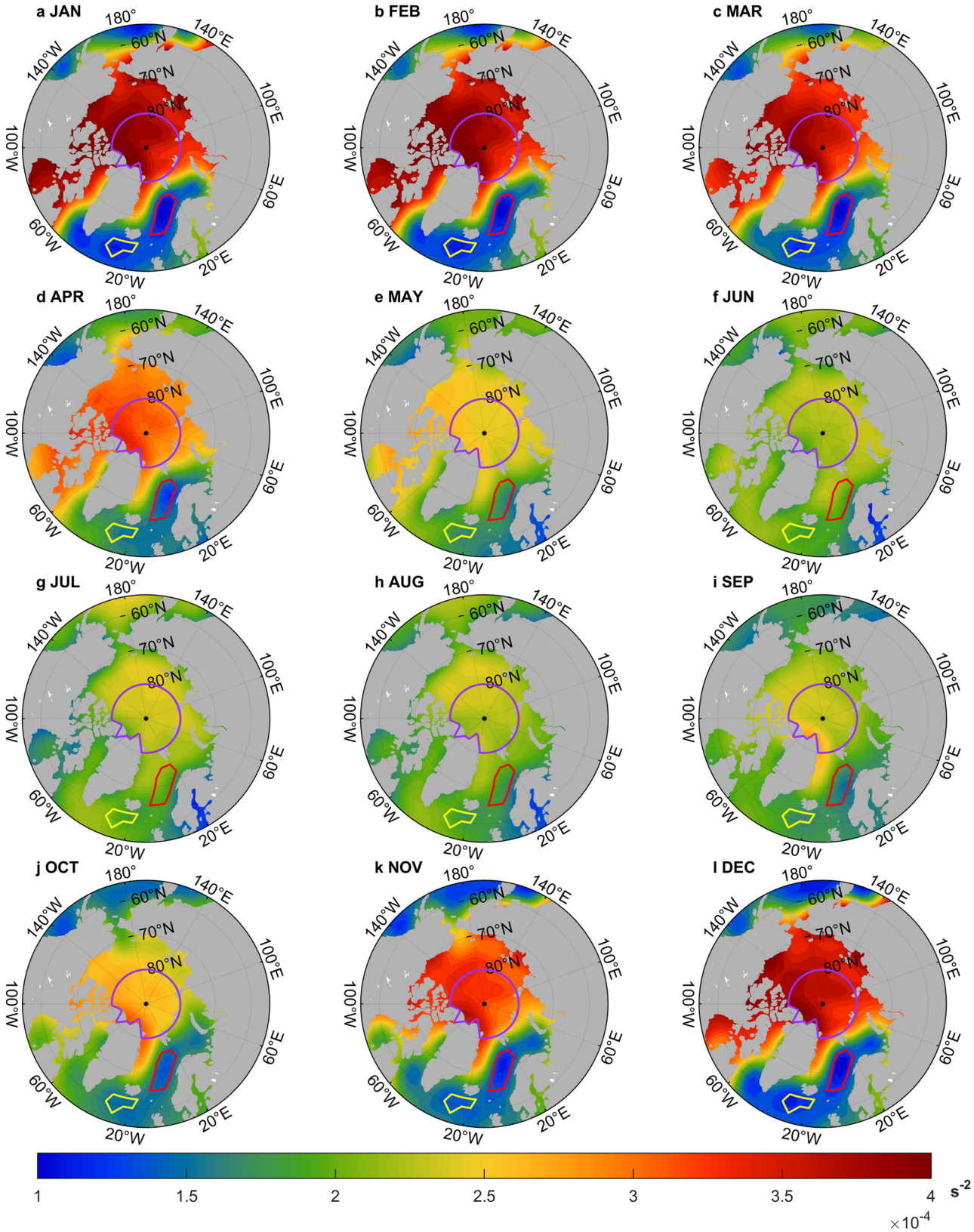

Fig. 1 Climatological monthly static stability (N^2) of the Arctic Mediterranean lower atmosphere averaged over 1979–2022 (unit: s^{-2}). The region enclosed by the purple line represents the Polar Region, the red line corresponds to Region-A, and the yellow line outlines Region-B.

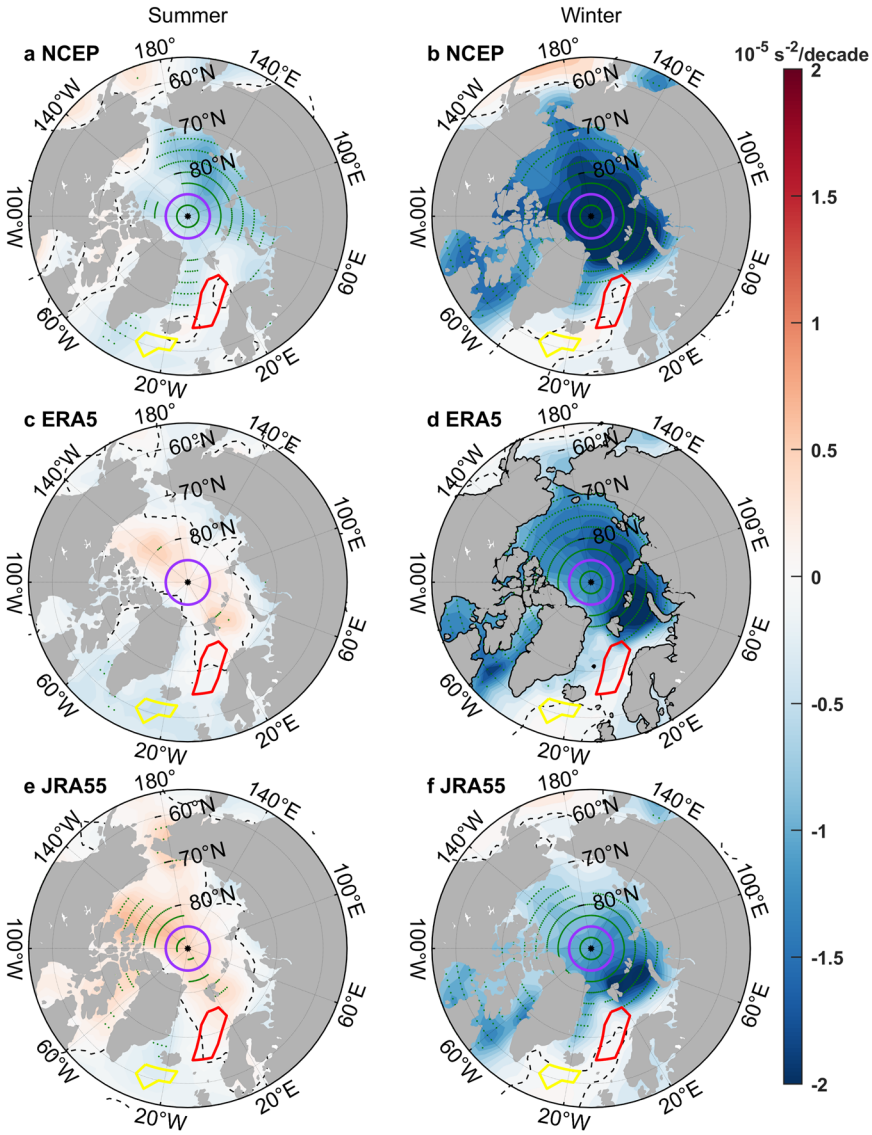

Fig. 2 Trends in lower atmospheric static stability over the Arctic Mediterranean (1979–2022). This figure presents the data from three reanalysis datasets: NCEP-R2 (**a**, **b**), ERA5 (**c**, **d**), and JRA-55 (**e**, **f**). **a**, **c**, **e** depict the summer trend, while **b**, **d**, **f** display the winter trend. The region enclosed by the purple line represents the Polar Region, the red line corresponds to Region-A, and the yellow line outlines Region-B. The zero contours are dashed. The green asterisks showstatistical significance at the 95% level. Shading unit: s^{-2} per decade.

currents[55–57]. The open ocean strongly releases heat, warming the lower atmosphere and reducing the stability[15,27,33,58,59]. This lower SSLA fosters conditions conducive to the acceleration of vertical movement[10,40,60].

In summer (June–August), the SSLA in the central Arctic Ocean significantly decreases due to the seasonal retreat of sea ice. The higher air temperature during this period results in lower static stability ($\sim 2.4 \times 10^{-4}\,s^{-2}$). Consequently, in the Norwegian Sea and the area south of Iceland, the heat flux into the atmosphere reaches its lowest levels during summer[57], leading to a higher SSLA ($\sim 2.0 \times 10^{-4}\,s^{-2}$). Consequently, the static stability in these regions exhibits notable uniformity. While spatial differences in SSLA are pronounced during the winter season, they become less apparent in the summer, a phenomenon explained by the minimal air-sea temperature difference between the Arctic Ocean and the Nordic Seas.

Based on the climatological SSLA of the Arctic Mediterranean in winter, we identified three representative regions, the Polar Region (north of 80°N), Region-A (over the Norwegian Sea) and Region-B (located south of Iceland). The Polar Region represents the ice-covered ocean with high SSLA, whereas Region-A and Region-B were selected based on N^2 values lower than $1.34 \times 10^{-4}\,s^{-2}$, a threshold set at two standard deviations from the spatial mean SSLA[27,61,62]. Although the selection criteria have some arbitrariness, the results are not sensitive to the criteria. Region-A and Region-B, both characterized by low SSLA values, exhibit distinctive underlying conditions. Region-A is heavily influenced by the Norwegian Atlantic Current[59,63], whereas Region-B is dominated by the recirculated North Atlantic Current water[61,64], so we discussed them separately.

Trend of atmospheric static stability from 1979 to 2022

In consideration of the seasonal cycle of stability, we study the trends in summer and winter separately.

As illustrated in Fig. 2a, b, the SSLA in the central Arctic Ocean represents declining trends based on NCEP-R2 data. In winter, a statistically significant reduction of $(-2.1 \pm 0.9) \times 10^{-5}\,s^{-2}$ per decade is observed with a confidence level of 95%. In summer, the reduction is $(-7.3 \pm 2.7) \times 10^{-6}\,s^{-2}$ per decade. The result is

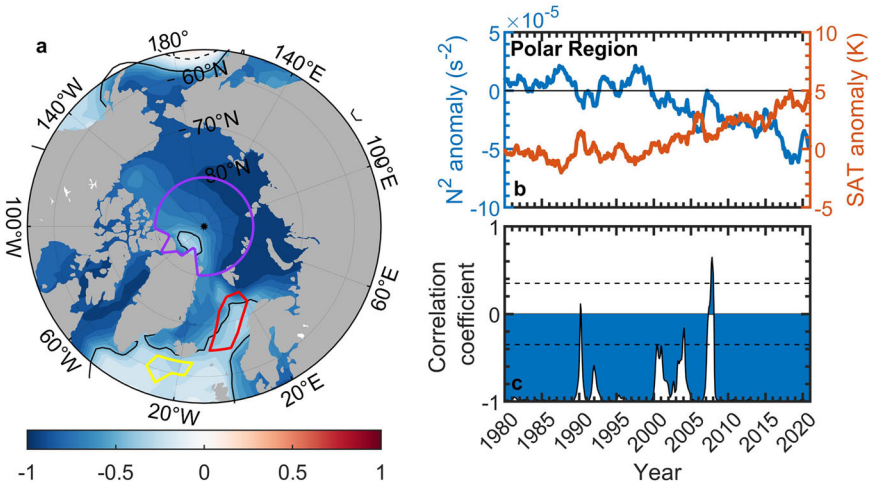

Fig. 3 The correlation between the monthly static stability (s^{-2}) of the lower atmosphere and surface air temperature anomaly (K), smoothed with a 13-month sliding average. a Spatial distribution of correlation coefficient of gridded N^2 and surface air temperature (SAT) anomaly. The region enclosed by the purple line represents the Polar Region, the red line corresponds to Region-A, and the yellow line outlines Region-B. Dashed zero contours are shown. The solid black line represents the critical correlation coefficient contours with a confidence level of 95%. **b** The 13-month averaged time series of N^2 (blue line) and SAT (red line) anomalies in the Polar Region. **c** The 13-month running correlation between N^2 and SAT anomalies in the Polar Region, smoothed with a 13-month sliding average. The black dashed line represents the critical correlation coefficient with a confidence level of 95%.

anticipated because of sea ice retreat and Arctic warming. Firstly, the sea surface air temperature in the Polar Region increased approximately 3 °C since the 1980s, closely associated with Arctic warming[31,32,34,36,65,66] directly leads to a decrease in SSLA with a correlation coefficient of −0.9 (Fig. 3). Secondly, the rapid decline of sea ice in summer has expanded the area of open water[28,32,33], and more solar radiation was absorbed by the ocean and subsequently released to atmosphere. The oceanic heating from the ocean weakened SSLA during fall and winter[15,28,33,46]. The combination of the two factors has led to a noticeable decline trend of SSLA in Arctic Ocean. The trend in winter is nearly two times that in summer, as the Arctic warming is more pronounced in winter[46]. Despite these trends, it's important to note that the SSLA in the central Arctic remains at a relatively high level compared to the climatological mean. This suggests that while a decline is evident, it has not exerted significant influence on vertical movement within the central Arctic.

It should be noticed that the summer trend revealed by ERA5 and JRA-55 datasets are different than that of NCEP-R2. SSLA, as determined from ERA5 data, indicates a subtle increasing trend, though it is statistically insignificant (Fig. 2c, d). SSLA calculated from JRA-55 data present an increase trend, $(6.2 \pm 1.4) \times 10^{-6}$ s^{-2} per decade, statistically significant at the 95% confidence level (Fig. 2e, f). The discrepancy only appeared in ice-covered regions and is specific to the summer season. Presumably, this may be caused by the different thermal boundary conditions in their assimilation models. However, no matter whether the static stability over the Arctic Ocean is decreasing or increasing in summer, the climatological SSLA in Arctic Ocean is high enough to dominate the stable atmosphere.

The trends of SSLA in Region-A and Region-B were not evidence in summer and winter. This is because these areas are ice-free all year round[56], and there is no obvious warming appearance to change the SSLA. In addition, the long-term trend of the heat fluxes in the Nordic Seas is not statistically significant[59] and they did not induce any significant trend in the regional SSLA.

Oscillatory variation in static stability

As shown in Fig. 4, the oscillatory variations in the SSLA over the three regions were quite consistently using different datasets. In the Polar Region, the average amplitude of oscillatory variations of SSLA in winter was ~1.95×10^{-5} s^{-2} (Fig. 4a, b), being negligible compared to the trend. In summer, the mean amplitude of oscillatory variation was ~9.80×10^{-6} s^{-2}. Due to the high climatological static stability in the Arctic, the oscillatory variations did not significantly reduce the static stability to trigger an unstable atmosphere.

In Region-A (Fig. 4c, d), the average amplitude of the oscillatory variation was ~9.18×10^{-6} s^{-2} in winter and ~6.19×10^{-6} s^{-2} in summer, respectively. In Region-B (Fig. 4e, f), the oscillatory variation was ~ 1.10×10^{-5} s^{-2} in winter and 1.02×10^{-5} s^{-2} in summer. The oscillatory over Region-A and Region-B in summer is weaker than that in winter because the lower SSLA appears in winter. During winter, when a negative oscillatory SSLA is superimposed on this already low background SSLA, it can lead to significantly reduced atmospheric stability, thereby weakening the damping effect of a stable atmosphere on small- and meso-scale systems[10]. Consequently, the oscillatory variations in SSLA within Region-A and Region-B assume an important role in influencing the vertical motion of the atmosphere, particularly during the winter season.

Mechanism of oscillated variation of atmospheric static stability

The variations in the SSLA over the Arctic Mediterranean mainly exhibited a trend and an oscillation variation. The trend is attributed to Arctic warming and the oscillated variation is related to Arctic Oscillation. As the oscillatory variation in the Polar Region is insignificant, the driving factor of the oscillated variations of SSLA in Region-A and Region-B are mainly discussed here. A 13-month running average of SSLA anomaly data and Arctic Oscillation index (AOI) were adopted to filter out seasonal and other high frequency variations. The relationship between AO and SSLA are clearly expressed in Fig. 5. The processes well studied are expressed by blue arrows, and processes revealed by this study are represented by red arrows.

The AO is the main atmospheric circulation pattern in the Northern Hemisphere, especially in winter[42,67]. When positive AO occurs, the atmospheric circulation and upward velocity surround Icelandic Low are all enhanced[57,68,69], and the oceanic circulation enhances thereby and drives a positive anomaly of SST in the regions influenced by warm current water, and vice versa[57,70–72].

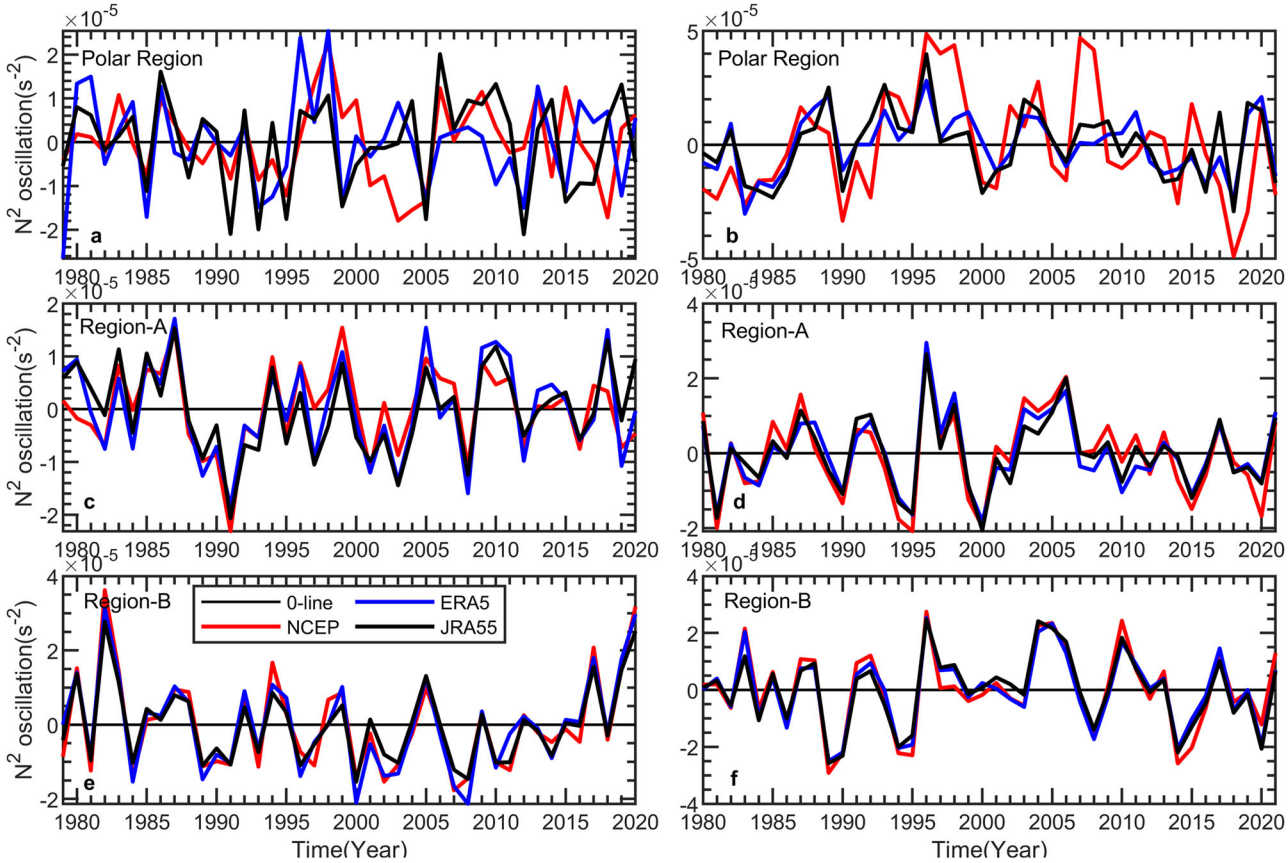

Fig. 4 Oscillatory variations in the static stability of the lower atmosphere across three regions. Panels (**a**), (**c**), and (**e**) represent the Polar Region, Region-A, and Region-B during summer, respectively, while panels (**b**), (**d**), and (**f**) depict the same regions in winter. The red line corresponds to NCEP-R2 results, the blue line represents ERA5 results, and the black line illustrates JRA-55 results. The thin black lines indicate the zero line.

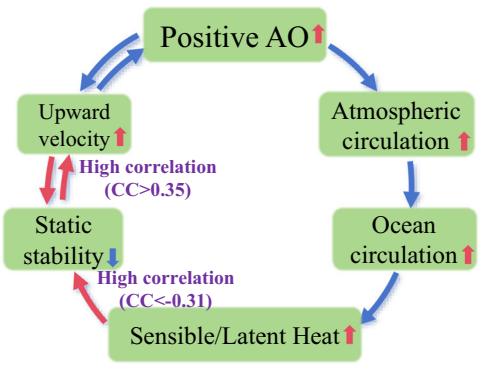

Fig. 5 Mechanism of lower atmosphere static stability variation. Blue long arrows depict established processes, while red long arrows highlight processes unveiled in this study. A straight short red arrow pointing upward indicates enhancement, and a straight short blue arrow pointing downward indicates attenuation.

A high correlation area of AOI with vertical velocity at 500 hPa around Icelandic Low exists (Fig. 6a), and the averaged vertical velocity and AOI (Fig. 6b) are close correlated negatively as shown in Fig. 6c with the correlation coefficient of −0.74 (at the 95% confidence level).

At the background of the high correlation between vertical velocity and AOI, they both are all correlated well with the SSLA. The correlation coefficients between AOI and the SSLA averaged in Region-A and Region-B are −0.50 and −0.31 and are significant at the 95% and 90% confidence level, respectively. The correlation coefficients of the averaged vertical velocity (blue line) shown in Fig. 6b with SSLA averaged in Region A and Region B are 0.47 and 0.35 (at the 95% and 90% confidence levels), respectively. Three possible driving factors related to the vertical velocity and N2 are discussed.

The first possibility is the advection of lower atmosphere from lower latitudinal region. Our result indicated that the SSLA in mid-latitude North Atlantic is very high, being not the source of the low SSLA in the study regions. The SSLA similar to the two regions is limited in a narrow zone around north of 50 °N, not supporting the import of low SSLA from mid-latitude (Fig. 7).

The second anticipated mechanism posits that upward velocity induces a reduction in SSLA by stretching the atmospheric column. The vertical advection extends the distance of the isentropic surface, resulting in a decrease in SSLA, as evidenced by the observed close correlation between them. Our observations indicate that the vertical velocity precedes the static stability by 1 day in Region-A (Fig. 8e).

The third possibility of SSLA correlated with vertical velocity is the heating from ocean surface. In the positive AO situation, ocean circulation enhances driven by enhanced atmospheric circulation, and the SST increase accordingly[73]. A portion of warmer North Atlantic Current enters Region-A and the other portion of it recirculates to the Region-B[74]. The warmer ocean surface heats the overlying atmosphere by sensible and latent heats[57,75]. Table 1 provides the summary statistics for correlations among regional average heat flux, stability, and other variables. As shown in Table 1, sensible/latent heat is highly correlated with SSLA. To explore the causal relationship, daily average data during the positive AO phase (1990–1994) were employed for lead-lag analysis (Fig. 8).

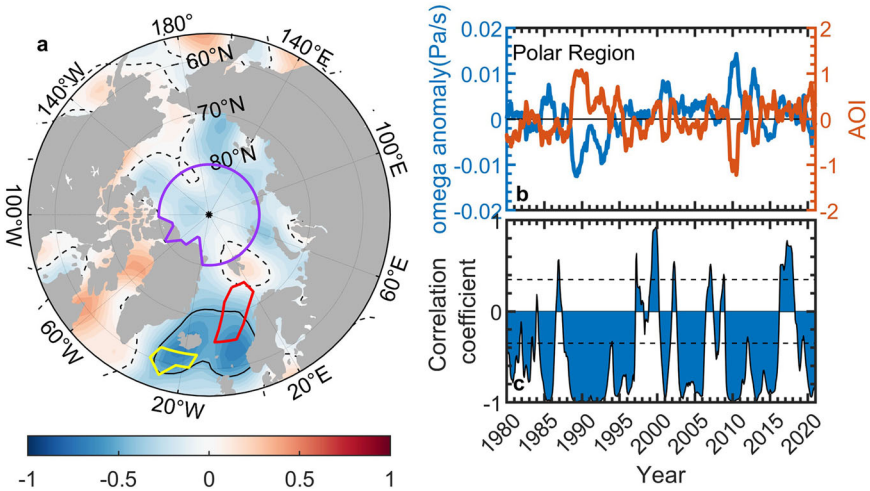

Fig. 6 The same as Fig. 3 but for vertical velocity (Pa s^{-1}) and the AOI. The region enclosed by the black line represents the High Correlation Region (HCR), whose correlation coefficient are lower than the critical one with a confidence level of 95%.

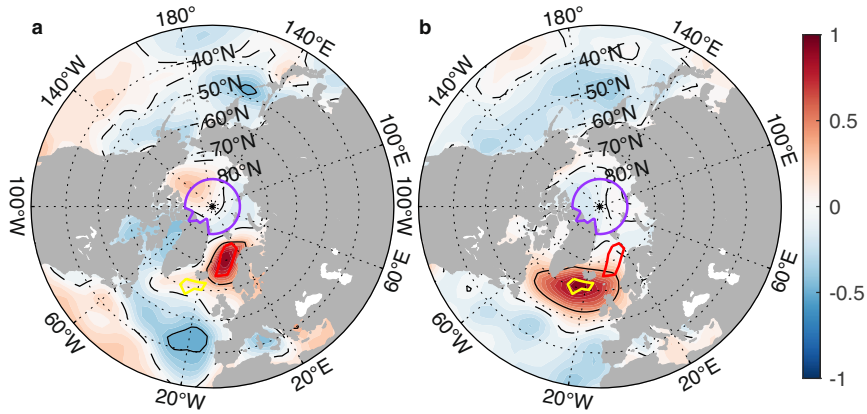

Fig. 7 Monthly gridded stability correlation with regional averages (Region-A and Region-B). Correlation between monthly gridded stability and regional averages in Region-A (**a**) and Region-B (**b**), smoothed with 13-month running average. The region enclosed by the purple line represents the Polar Region, the red line corresponds to Region-A, and the yellow line outlines Region-B. Dashed zero contours are shown. The solid black line represents the critical correlation coefficient contours with a confidence level of 95%.

The results reveal zero lag days, indicating an instantaneous association and direct influence between heat flux and SSLA. Therefore, the third proposed mechanism suggests a robust connection between SSLA variation and sea surface heating.

According to Fig. 8e and f, the relationship between vertical velocity and static stability varies across regions. In Region-A, vertical velocity leads static stability by one day. Conversely, in Region-B, static stability leads vertical velocity by two days. The lead of vertical velocity to SSLA signifies that the vertical velocity modifies the static stability through vertical stretching of the air column. This stretching weakens static stability, further amplifying vertical velocity in a positive feedback loop. Conversely, the lag of vertical velocity to SSLA indicates that stability is initially altered by surface heating. The weakened stability facilitates the enhancement of vertical velocity, establishing a positive feedback loop through surface heating. The SSLA variation due to vertical stretching is an internal atmospheric process, whereas that resulting from surface heating belongs to the coupled process of air-sea interaction. We contend that the natural process may involve both driving factors. In Region-A, the internal atmospheric process dominates, while in Region-B, air-sea coupling takes precedence.

The aforementioned results indicate that a decrease in static stability corresponds to an increase in vertical velocity, thereby contributing to the development of the positive phase of the AO. This finding aligns with previous research[57], identifying a positive feedback region in the North Atlantic that demonstrates the positive impact of surface heating on AO. The positive feedback region contributes to the oscillated variation of AO.

This study enhances our understanding of the AO variation mechanism by revealing that the positive feedback from ocean heating to AO operates through SSLA. Importantly, the results suggest that this positive feedback is not infinite, concluding when static stability approaches zero.

DISCUSSION

In this comprehensive exploration of SSLA in the Arctic Mediterranean, we gained insights into the distinctive patterns and mechanisms governing SSLA.

Firstly, in the Arctic Ocean, SSLA variations predominantly displayed a substantial decreasing trend in both summer and winter, accompanied by weak oscillatory variations. This trend was primarily attributed to Arctic warming and sea ice retreat. Arctic warming led to higher air temperature in the lower atmosphere,

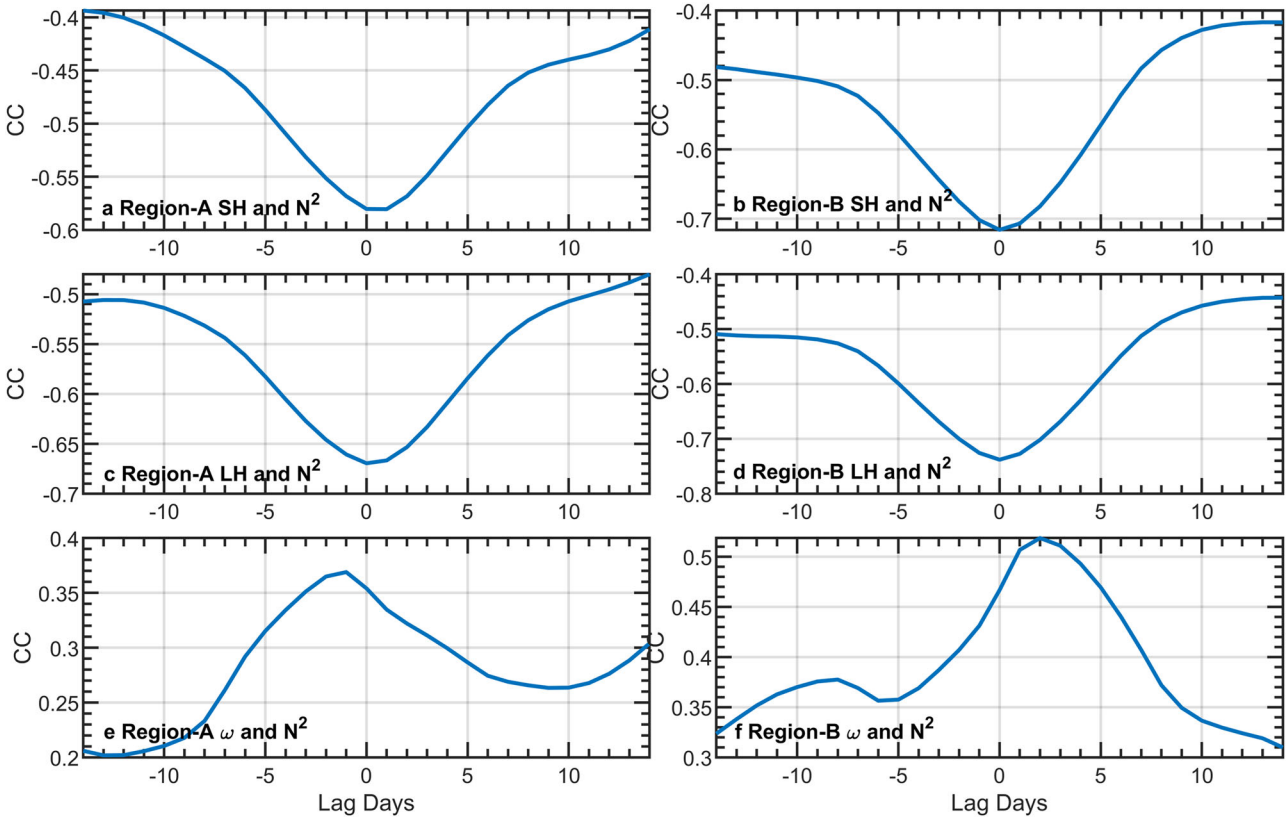

Fig. 8 Lagged correlation of fluxes and velocity with stability (Region-A/B) during positive ArcticOscillation (1990–1994). The left panel (**a**, **c**, **e**) focuses on Region-A, while the right panel (**b**, **d**, **f**) examines Region-B. Negative lag days indicate that sensible (**a**, **b**)/latent (**c**, **d**) heat fluxes (SH/LH) and vertical velocity (ω, (**e**, **f**)) precede the static stability. Conversely, positive lag days indicate anadvancement of the static stability. The correlation coefficients (CC) are statistical significance at a confidence level of 90%.

Table 1. Correlation coefficients among regional average variables.

CC	Region-A	Region-B
ω and N^2	0.28	0.42
SH and N^2	−0.31	−0.52
LH and N^2	−0.41	−0.58

(ω) vertical velocity, *SH/LH* Sensible/Latent Heat Fluxes. The correlation coefficients (CC) are statistical significance at a confidence level of 90%.

while the sea ice retreat resulted in increased open water and enhanced ocean-to-atmosphere heat release. Both factors significantly contributed to the diminishing SSLA. The declining trend was particularly noteworthy during winter, with a reduction of approximately 13 ± 5% over the past two decades. Despite this reduction, the atmosphere retains a high degree of stability, underscoring the persistent background static stability.

Secondly, Region-A and Region-B are ice-free areas and exhibit a low background SSLA. The SSLA trends were not significant in both summer and winter. However, the oscillatory variations in SSLA in these regions were considerably more pronounced than the trends. The amplitude of SSLA variation exceeded $6.19 \times 10^{-6}\,s^{-2}$, reaching 26% of the background value. Consequently, the role of oscillatory SSLA is notably significant. SSLA is highly correlated with AO index and vertical velocity, indicating a close relationship among them. The oscillatory variations were suggested to be linked to the warm current, closely related to the AO. In a positive AO phase, atmospheric and oceanic circulations intensify, leading to a warmer sea surface. Subsequently, the heating from underlying surface drives the weakening of SSLA.

Thirdly, the lead-lag correlation results reveal that in Region-A, vertical velocity leads static stability by one day, indicating a positive feedback loop through vertical stretching of the air column, weakening stability and enhancing vertical velocity. In Region-B, static stability precedes vertical velocity by two days, indicating a surface heating dominate process. SSLA variation from vertical stretching is an internal atmospheric process, while surface heating involves air-sea interaction. Both factors contribute to the natural process, with internal processes dominant in Region-A and air-sea coupling dominate in Region-B. This mechanism suggests that the weakened SSLA enhances vertical velocity, contributing to the positive phase of AO. This aligns with the previous study by ref. [57].

The contribution of our study lies in revealing that the positive feedback of ocean heating to AO operates through SSLA, offering a comprehensive understanding of the AO variation mechanism. Importantly, the results indicate that this positive feedback is not infinite, which will terminate when static stability tends toward zero.

METHODS

Reanalysis data

The data utilized in this study were obtained from daily and monthly average reanalysis datasets, namely NCEP-R2, ERA5, and JRA-55. These datasets included daily and monthly average grid data for various isobaric surface parameters, such as air temperature, relative humidity, horizontal wind velocity, vertical velocity and geopotential height. Additionally, single-level data for

variables like sea surface temperature, surface air temperature and sensible/latent heat flux, as well as the Arctic Oscillation index data, were also incorporated. The horizontal resolution of the grid data is 2.5° × 2.5°, and the duration is 44 years from January 1979 to December 2022. The study area was mainly north of 50 °N.

Static stability calculation

The vertical motion in the atmosphere falls into two broad categories: systematic vertical motion and convective vertical motion. The static stability discussed in this paper is a parameter closely related to convective vertical motion.

The gas block method is often used to identify the static stability of the atmosphere and to analyze the vertical movement of a gas block. Combined with the atmospheric state equation, the vertical motion equation can be obtained using the following static approximation:

$$\frac{dw}{dt} = -g - \frac{1}{\rho}\frac{\partial p}{\partial z} = g\frac{\overline{\rho} - \rho}{\rho} = \frac{g}{\overline{T}}(\gamma - \gamma_d)z \tag{1}$$

where g is acceleration of gravity, T is the air temperature, p is the atmospheric pressure, z is the vertical coordinate, w is the vertical velocity, ρ is the the density of the atmosphere, γ is the vertical temperature lapse rate, γ_d is the dry air temperature vertical lapse rate, and - denotes a parameter of the ambient atmosphere. The Brunt-Väisälä frequency N^2 was introduced to characterize the static stability[8,39,40]:

$$N = \left[\frac{g}{\overline{T}}(\gamma_d - \gamma)\right] = \left(\frac{g}{\overline{\theta}}\frac{\partial\overline{\theta}}{\partial z}\right)^{\frac{1}{2}} \tag{2}$$

The potential temperature (θ) was calculated as follows:

$$\theta = T\left(\frac{1000}{p}\right)^{\frac{R}{C_p}} \tag{3}$$

where R is the ideal gas constant, and C_p is the specific heat at constant pressure. In this case, the vertical kinematics equation can be rewritten as

$$\frac{d^2z}{dt^2} + N^2 z = 0 \tag{4}$$

When N^2>0, Eq. (4) is the vibration equation, and the vibration frequency is N. When the atmosphere is stable, the air block vibrates up and down at the equilibrium position. The larger the magnitude of N is, the higher the vibration frequency is, the more stable the atmosphere is, and the more difficult it is for the air block to deviate from the equilibrium position.

Significance of correlation

For a completely random time series, the degree of freedom is data length minus 2. However, many time series in our calculations are not completely random, especially those that cover seasonal and interannual variations. When we process the data, we often use filtering and other methods to change the degree of freedom in order to get the special frequency band signals we pay attention to. Therefore, it is particularly important to calculate the equivalent degree of freedom when testing the significance of correlation coefficients. The statistical significance of the correlation coefficient accounts for the autocorrelation in the time series by using an effective degree of freedom N^*[31]:

$$N^* = N\frac{1 - r_1 r_2}{1 + r_1 r_2} \tag{5}$$

where N is the sample size of the time series, and r_1 and r_2 are the lag-1 autocorrelation coefficients of each variable. In this study, the confidence level is tested using the two-tailed Student's t-test.

Running correlation

The running correlation coefficient (RCC) between two time series were calculated to reveal the variation of the correlations with time.

The RCC, $R_c(i)$ between two time series, X_k and Y_k, centered at i_{th} month with the window length of ±n is expressed as ref. [76].

$$R_c(i) = \frac{\sum_{k=i-n}^{i+n}(X_k - \overline{X})(Y_k - \overline{Y})}{\sqrt{\sum_{k=i-n}^{i+n}(X_k - \overline{X})^2}\sqrt{\sum_{k=i-n}^{i+n}(Y_k - \overline{Y})^2}}, i = 1 + n, \cdots, N - n \tag{6}$$

Note that $\overline{X}$ and $\overline{Y}$ are not the means inside the window, but the means for all of the data, based on the suggestion of ref. [76]. In this study, n was taken as 6 months. The RCC was obtained by moving the window month by month.

DATA AVAILABILITY

In this study, all reanalysis data were sourced from publicly available platforms. Monthly and daily data for air temperature, relative humidity, horizontal wind velocity, vertical velocity and geopotential height on isobaric surface were obtained from the NCEP-R2(https://downloads.psl.noaa.gov/Datasets/ncep.reanalysis2/), ERA5 (https://cds.climate.copernicus.eu/cdsapp#!/dataset/reanalysis-era5-pressure-levels-monthly-means?tab=doc and https://cds.climate.copernicus.eu/cdsapp#!/dataset/reanalysis-era5-pressure-levels?tab=overview) and JRA-55. The Arctic Oscillation index data is accessible at https://www.cpc.ncep.noaa.gov/products/precip/CWlink/daily_ao_index/ao.shtml. Single-level data for variables like sea surface temperature, surface air temperature and sensible/latent heat flux were obtained from the NCEP-R2 (https://psl.noaa.gov/data/gridded/data.noaa.oisst.v2.html, https://downloads.psl.noaa.gov/Datasets/ncep.reanalysis2/Monthlies/gaussian_grid/), ERA5 (https://cds.climate.copernicus.eu/cdsapp#!/dataset/reanalysis-era5-single-levels-monthly-means?tab=form) and JRA-55. As of February 3, 2024, successful access to all sites has been confirmed.

CODE AVAILABILITY

The data reading and processing codes are available from https://doi.org/10.5281/zenodo.10468030. All programs in this study are implemented based on Matlab R2022b.

Received: 17 May 2023; Accepted: 11 January 2024;
Published online: 24 January 2024

REFERENCES

1. Fleagle, R. G. & Businger, J. A. *An Introduction To Atmospheric Physics* 52–54 (Academic Press), (1981).
2. Salby, M. L. *Fundamentals Of Atmospheric Physics* 8–16 (Elsevier), (1996).
3. Crook, N. A. Sensitivity of moist convection forced by boundary layer processes to low-level thermodynamic fields. *Mon. Weather Rev.* **124**, 1767–1785 (1996).
4. Sherwood, S. C., Roca, R., Weckwerth, T. M. & Andronova, N. G. Tropospheric water vapor, convection, and climate. *Rev. Geophys.* **48**, RG2001 (2010).
5. Emanuel, K. A., David Neelin, J. & Bretherton, C. S. On large-scale circulations in convecting atmospheres. *Q. J. R. Meteorol. Soc.* **120**, 1111–1143 (1994).
6. Roland, S. *Meteorology For Scientists And Engineers, 3rd Ed.* 119–158 http://www.eos.ubc.ca/books/Practical_Meteorology/ (Brooks/Cole), (2000).
7. Liu, W., Tian, W., Shu, J., Zhang, J. & Hu, D. Effects of quasi-biennual oscillation on tropical tropopause and deep convective activities. *Adv. Earth Sci.* **30**, 724–736 (2015).
8. Durran, D. R. & Klemp, J. B. On the effects of moisture on the Brunt-Väisälä. *Frequency. J. Atmos. Sci.* **39**, 2152–2158 (1982).
9. Frierson, D. M. W. Robust increases in midlatitude static stability in simulations of global warming. *Geophys. Res. Lett.* **33**, L24816 (2006).
10. Sumner, E. J. The significance of vertical stability in synoptic development. *Q. J. R. Meteorol. Soc.* **76**, 384–392 (1950).
11. Staley, D. O. & Gall, R. L. On the wavelength of maximum baroclinic instability. *J. Atmos. Sci.* **34**, 1679–1688 (1977).
12. Juckes, M. N. The static stability of the midlatitude troposphere: the relevance of moisture. *J. Atmos. Sci.* **57**, 3050–3057 (2000).

13. Hoskins, B. & Wang, B. *Large-Scale Atmospheric Dynamics* 357–365 (Springer), (2006).
14. Frierson, D. M. W., Lu, J. & Chen, G. Width of the Hadley cell in simple and comprehensive general circulation models. *Geophys. Res. Lett.* **34**, L18804 (2007).
15. Jaiser, R., Dethloff, K., Handorf, D., Rinke, A. & Cohen, J. Impact of sea ice cover changes on the Northern Hemisphere atmospheric winter circulation. *Tellus A* **64**, 497 (2012).
16. Rinke, A., Dethloff, K., Dorn, W., Handorf, D. & Moore, J. C. Simulated Arctic atmospheric feedbacks associated with late summer sea ice anomalies. *J. Geophys. Res.* **118**, 7698–7714 (2013).
17. Vihma, T. Effects of Arctic sea ice decline on weather and climate: a review. *Surv. Geophys.* **35**, 1175–1214 (2014).
18. Özsoy, E. *Internal Waves. In: Geophysical Fluid Dynamics II (ed. Özsoy, E.)* 101–171 (Springer, Cham), (2021).
19. Yoshiki, M. & Sato, K. A statistical study of gravity waves in the polar regions based on operational radiosonde data. *J. Geophys. Res.* **105**, 17995–18011 (2000).
20. McHugh, J. P. Incidence and reflection of internal waves and wave-induced currents at a jump in buoyancy frequency. *Nonlin. Process. Geophys.* **22**, 259–274 (2015).
21. Klein, S. A. & Hartmann, D. L. The seasonal cycle of low stratiform clouds. *J. Clim.* **6**, 1587–1606 (1993).
22. Curry, J. A. Interactions among aerosols, clouds, and climate of the Arctic Ocean. *Sci. Total Environ.* **160**, 777–791 (1995).
23. Kay, J. E. & Gettelman, A. Cloud influence on and response to seasonal Arctic sea ice loss. *J. Geophys. Res.* **114**, D18204 (2009).
24. Kay, J. E., Raeder, K., Gettelman, A. & Anderson, J. The boundary layer response to recent Arctic sea ice loss and implications for high-latitude climate feedbacks. *J. Clim.* **24**, 428–447 (2011).
25. Gray, W. M. Tropical cyclone genesis in the western North Pacific. *J. Meteorol. Soc. Jpn.* **55**, 465–482 (1977).
26. Crawford, A. D., Lukovich, J. V., McCrystall, M. R., Stroeve, J. C. & Barber, D. G. Reduced sea ice enhances intensification of winter storms over the Arctic Ocean. *J. Clim.* **35**, 3353–3370 (2022).
27. Francis, J. A., Chan, W., Leathers, D. J., Miller, J. R. & Veron, D. E. Winter Northern Hemisphere weather patterns remember summer Arctic sea-ice extent. *Geophys. Res. Lett.* **36**, L07503 (2009).
28. Schweiger, A. J., Lindsay, R. W., Vavrus, S. & Francis, J. A. Relationships between Arctic sea ice and clouds during autumn. *J. Clim.* **21**, 4799–4810 (2008).
29. Screen, J. & Simmonds, I. The central role of diminishing sea ice in recent Arctic temperature amplification. *Nature* **464**, 1334–1337 (2010).
30. Sedlar, J. et al. A transitioning Arctic surface energy budget: the impacts of solar zenith angle, surface albedo and cloud radiative forcing. *Clim. Dyn.* **37**, 1643–1660 (2011).
31. Serreze, M. C., Barrett, A. P., Stroeve, J. C., Kindig, D. N. & Holland, M. M. The emergence of surface-based Arctic amplification. *Cryosphere* **3**, 11–19 (2009).
32. Deser, C., Tomas, R., Alexander, M. & Lawrence, D. The seasonal atmospheric response to projected Arctic sea ice loss in the late twenty-first century. *J. Clim.* **23**, 333–351 (2010).
33. Overland, J. E. & Wang, M. Large-scale atmospheric circulation changes associated with the recent loss of Arctic sea ice. *Tellus Ser. A-Dyn. Meteorol. Oceanogr.* **62**, 1–9 (2010).
34. Screen, J. A. & Simmonds, I. Increasing fall-winter energy loss from the Arctic Ocean and its role in Arctic temperature amplification. *Geophys. Res. Lett.* **37**, L16707 (2010).
35. Kurtz, N. T., Markus, T., Farrell, S. L., Worthern, D. L. & Boisvert, L. N. Observations of recent Arctic sea ice volume loss and its impact on ocean-atmosphere energy exchange and ice production. *J. Geophys. Res.* **116**, C04015 (2011).
36. Serreze, M. C. & Barry, R. G. Processes and impacts of Arctic amplification: a research synthesis. *Glob. Planet. Change* **77**, 85–96 (2011).
37. Screen, J. A., Simmonds, I., Deser, C. & Tomas, R. The atmospheric response to three decades of observed Arctic sea ice loss. *J. Clim.* **26**, 1230–1248 (2013).
38. Kumar, A. et al. Contribution of sea ice loss to Arctic amplification. *Geophys. Res. Lett.* **37**, L21701 (2010).
39. Strey, S. T., Chapman, W. L. & Walsh, J. E. The 2007 sea ice minimum: impacts on the Northern Hemisphere atmosphere in late autumn and early winter. *J. Geophys. Res.* **115**, D23103 (2010).
40. Porter, D. F., Cassano, J. J. & Serreze, M. C. Local and large-scale atmospheric responses to reduced Arctic sea ice and ocean warming in the WRF model. *J. Geophys. Res.* **117**, D11115 (2012).
41. Thompson, D. W. J. & Wallace, J. M. The Arctic oscillation signature in the wintertime geopotential height and temperature fields. *Geophys. Res. Lett.* **25**, 1297–1300 (1998).
42. Thompson, D. W. J. & Wallace, J. M. Regional climate impacts of the Northern Hemisphere annular mode. *Science* **293**, 85–89 (2001).
43. Wallace, J. M. & Thompson, D. W. J. The Pacific center of action of the northern hemisphere annular mode: real or artifact? *J. Clim.* **15**, 1987–1991 (2002).
44. Ambaum, M. H. P., Hoskins, B. J. & Stephenson, D. B. Arctic oscillation or north atlantic oscillation? *J. Clim.* **14**, 3495–3507 (2001).
45. Zhao, J., Cao, Y. & Shi, J. Spatial variation of the Arctic Oscillation and its long-term change. *Tellus Ser. A-Dyn. Meteorol. Oceanogr.* **62**, 661–672 (2010).
46. Dai, A., Luo, D., Song, M. & Liu, J. Arctic amplification is caused by sea-ice loss under increasing CO^2. *Nat. Commun.* **10**, 121 (2019).
47. Gettelman, A. et al. The extratropical upper troposphere and lower stratosphere. *Rev. Geophys.* **49**, RG3003 (2011).
48. Rinke, A., Maslowski, W., Dethloff, K. & Clement, J. Influence of sea ice on the atmosphere: a study with an Arctic atmospheric regional climate model. *J. Geophys. Res. Atmos.* **111**, D16 (2006).
49. Serreze, M. C., Kahl, J. D. & Schnell, R. C. Low-level temperature inversions of the Eurasian Arctic and comparisons with Soviet drifting station data. *J. Clim.* **5**, 615–629 (1992).
50. Palo, T., Vihma, T., Jaagus, J. & Jakobson, E. Observations of temperature inversions over central Arctic sea ice in summer. *Q. J. R. Meteorol. Soc.* **143**, 2741–2754 (2017).
51. Boe, J., Hall, A. & Qu, X. Current GCMs' unrealistic negative feedback in the Arctic. *J. Clim.* **22**, 4682–4695 (2009).
52. Shahi, S., Abermann, J., Heinrich, G., Prinz, R. & Schöner, W. Regional variability and trends of temperature inversions in Greenland. *J. Clim.* **33**, 9391–9407 (2020).
53. Wassmann, P. Vernal export and retention of biogenic matter in the northeastern North Atlantic and adjacent Arctic Ocean: the role of the Norwegian Atlantic Current and topography. *Mem. Natl Inst. Polar Res.* **54**, 377–392 (2001).
54. Hansen, B. & Østerhus, S. North atlantic-nordic seas exchanges. *Prog. Oceanogr.* **45**, 109–208 (2000).
55. Karpuz, N. K. & Jansen, E. A high-resolution diatom record of the last deglaciation from the SE Norwegian Sea: documentation of rapid climatic changes. *Paleoceanography* **7**, 499–520 (1992).
56. Kvingedal, B. Sea-ice extent and variability in the Nordic Seas, 1967–2002. *Geophys. Monogr. Ser.* **158**, 39–49 (2005).
57. Zhao, J., Drinkwater, K. & Wang, X. Positive and negative feedbacks related to the Arctic Oscillation revealed by air-sea heat fluxes. *Tellus Ser. A-Dyn. Meteorol. Oceanogr.* **71**, 1–21 (2019).
58. Stroeve, J. C. et al. Sea ice response to an extreme negative phase of the Arctic Oscillation during winter 2009/2010. *Geophys. Res. Lett.* **38**, L02502 (2011).
59. Smedsrud, L. H. et al. Nordic seas heat loss, atlantic inflow, and arctic sea ice cover over the last century. *Rev. Geophys.* **60**, e2020RG000725 (2022).
60. Coulter, R. L. & Martin, T. J. Effects of stability on the profiles of vertical velocity and its variance in katabatic flow. *Bound. Layer. Meteor.* **81**, 23–33 (1996).
61. Altman, D. G. & Bland, J. M. Standard deviations and standard errors. *Bmj* **331**, 903 (2005).
62. Stark, J. L. et al. Solution structure and function of YndB, an AHSA1 protein from *Bacillus subtilis*. *Proteins: Struct. Funct. Bioinf.* **78**, 3328–3340 (2010).
63. Mauritzen, C. Production of dense overflow waters feeding the North Atlantic across the Greenland-Scotland Ridge. Part 1: evidence for a revised circulation scheme. *Deep Sea Res. 1 Oceanogr. Res. Pap.* **43**, 769–806 (1996).
64. Bersch, M. North Atlantic Oscillation-induced changes of the upper layer circulation in the northern North Atlantic Ocean. *J. Geophys. Res. Oceans* **107**, 20–1 (2002).
65. Higgins, M. E. & Cassano, J. J. Impacts of reduced sea ice on winter Arctic atmospheric circulation, precipitation, and temperature. *J. Geophys. Res.* **114**, D16107 (2009).
66. Screen, J. A., Deser, C. & Simmonds, I. Local and remote controls on observed Arctic warming. *Geophys. Res. Lett.* **39**, L10709 (2012).
67. Chen, F. et al. Rapid warming in mid-latitude central Asia for the past 100 years. *Front. Earth Sci. China* **3**, 42–50 (2009).
68. Turner, J. et al. An Arctic and Antarctic perspective on recent climate change. *Int. J. Climatol.* **27**, 277–293 (2006).
69. Armitage, T. W. K. et al. Arctic sea level and surface circulation response to the arctic oscillation. *Geophys. Res. Lett.* **45**, 6576–6584 (2018).
70. Bjerknes, J. *Atlantic Air-Sea Interaction. In: Advances in geophysics* (ed. Landsberg, H. E. and Van Mieghem, J.) 1–82. (Elsevier), (1964).
71. Deser, C. & Timlin, M. S. Atmosphere-ocean interaction on weekly time scales in the North Atlantic and Pacific. *J. Clim.* **10**, 393–408 (1997).
72. Dickson, R. R. et al. The Arctic response to the North Atlantic Oscillation. *J. Clim.* **13**, 2671–2696 (2000).
73. Davis, B. A. & Brewer, S. Orbital forcing and role of the latitudinal insolation/temperature gradient. *Clim. Dyn.* **32**, 143–165 (2009).
74. Risebrobakken, B. et al. Buoyancy forcing: a key driver of northern North Atlantic sea surface temperature variability across multiple timescales. *Clim. Past* **19**, 1101–1123 (2023).

75. Piechura, J., Osiński, R., Petelski, T. & Wozniak, S. B. Heat and salt fluxes in the West Spitsbergen Current area in summer. *Oceanologia* **44**, 307–321 (2002).
76. Zhao, J., Cao, Y. & Wang, X. The physical significance of the synthetic running correlation coefficient and its applications in oceanic and atmospheric studies. *J. Ocean Univ. China* **17**, 451–460 (2018).

ACKNOWLEDGEMENTS

This study was supported by the National Basic Research Program of China (41976022) and the Key Project of Chinese Natural Science Foundation (41941012).

AUTHOR CONTRIBUTIONS

X.W.: methodology, formal analysis, data curation, writing—original draft, writing—review and editing, and visualization; J.P.Z.: conceptualization, supervision, methodology, writing—review and editing, and funding acquisition. All authors reviewed the manuscript.

COMPETING INTERESTS

The authors declare no competing interests.

ADDITIONAL INFORMATION

Correspondence and requests for materials should be addressed to Jinping Zhao.

Reprints and permission information is available at http://www.nature.com/reprints

Publisher's note Springer Nature remains neutral with regard to jurisdictional claims in published maps and institutional affiliations.